Static analysis of FGM cylinders by a mesh-free method

M. Foroutan*[1], R. Moradi-Dastjerdi[2], and R. Sotoodeh-Bahreini[1]

[1]*Mechanical Engineering Department, Razi University, Kermanshah, Iran*
[2]*Young Researchers Club, Khomeinishahr Branch, Islamic Azad University, Khomeinishahr, Iran*

(Received July 15, 2010, Revised January 02, 2011, Accepted October 11, 2011)

Abstract. In this paper static analysis of FGM cylinders subjected to internal and external pressure was carried out by a mesh-free method. In this analysis MLS shape functions are used for approximation of displacement field in the weak form of equilibrium equation and essential boundary conditions are imposed by transformation method. Mechanical properties of cylinders were assumed to be variable in the radial direction. Two types of cylinders were analyzed in this work. At first cylinders with infinite length were considered and results obtained for these cylinders were compared with analytical solutions and a very good agreement was seen between them. Then the proposed mesh-free method was used for analysis of cylinders with finite length and two different types of boundary conditions. Results obtained from these analyses were compared with results of finite element analyses and a very good agreement was seen between them.

Keywords: FGM; cylinder; stress; mesh-free; MLS shape function; FEM.

1. Introduction

Functionally graded materials were introduced for the first time by the material scientists as heat resistant materials for use in space planes and nuclear reactors. Recently, large amount of researches about application of these materials in wide range of industries such as dental and orthopedic implants, energy conversion, heat generators and sensors have been carried out. Additional potential applications of FGMs include their use as interfacial zones to improve the bonding strength and to reduce residual stresses in bonded dissimilar materials and as wear resistant layers such as gears, cams ball and roller bearings and machine tools. FGMs are the combination of two different materials, ceramic and metal. The volume fraction of these materials vary uniformly along a certain direction(s). Therefore FGMs have a non uniform microstructure and a continuously variable macrostructure.

Nowadays stress analysis of FGM pressure vessels is an important research field. Horgan and Chan (1999) presented an exact solution for static analysis of FGM pressure vessels and disks. Tutuncu and Ozturk (2001) analyzed FGM cylinders and spheres subjected to internal pressure by infinitesimal elasticity theory. Jabbari *et al*. (2006) presented a solution for thermal and mechanical stresses in FGM hollow cylinders. In another work Tutuncu (2007) introduced a power series solutions for stress and displacements in FGM cylindrical vessels. Li and Peng (2009) introduced a new method for stress analysis of FGM cylinders with arbitrarily varying material properties. Tutuncu and Temel (2009) determined axisymmetric displacements and stresses in FGM hollow cylinders and disks using complementary functions method.

In all of the above mentioned works analytical methods was used for stress analysis. Also in all of

* Corresponding author, Ph.D., E-mail: foroutan@razi.ac.ir

these works there aren't any essential boundary conditions. For stress analysis of FGM cylinders with finite length, there are some essential boundary conditions. These types of boundary conditions cause analytical methods to be more complex. Therefore, numerical methods are a good alternative for stress analysis of FGM cylinders with finite length including essential boundary conditions. Sladek *et al.* (2003) proposed a computational method for transient heat conduction analysis in continuously nonhomogeneous functionally graded materials (FGM). The method is based on the local boundary integral equations with moving least square approximation of the temperature and heat flux. Askari *et al.* (2009) carried out dynamic analysis of FGM cylinders with finite length subjected to impact load by the finite element method. Ching and Yen (2005) determined stresses in FGM cylinders subjected to internal pressure by the MLPG method. Gilhooley *et al.* (2008) used MLPG method for static and dynamic analysis of orthotropic FGM rotary disks and cylinders subjected to internal pressure. Sladek *et al.* (2008) developed LIE formulation for axisymmetric problem and determined stresses in FGM cylinders by a mesh-free method. Zhao and Liew (2010) presented the buckling response of functionally graded ceramic-metal cylindrical shell panels under axial compression and thermal load. The formulation is based on the first-order shear deformation shell theory and element-free *kp*-Ritz method.

In the present work a different mesh-free method was used for static analysis of FGM cylinders subjected to internal and external pressures. In this analysis MLS shape functions are used for the approximation of displacement field in the weak form of equilibrium equation and essential boundary conditions are imposed by transformation method. Results obtained from the proposed model for cylinders with infinite length were compared with exact solution. Also results obtained for cylinders with finite length were compared with results of the finite element analysis.

2. Governing equations

According to virtual work principle

$$\int_{\Omega} \boldsymbol{\sigma}.\delta(\boldsymbol{\varepsilon})dv - \int_{\Gamma} \mathbf{F}.\delta\mathbf{u}\,ds = 0 \tag{1}$$

Where $\boldsymbol{\sigma}$, $\boldsymbol{\varepsilon}$, $\mathbf{F}$ and $\mathbf{u}$ are stress vector, strain vector, traction vector and displacement vector respectively. Γ is a part of boundary of domain Ω on which traction $\mathbf{F}$ is applied. For axisymmetric problems stress and strain vectors are as follows

$$\boldsymbol{\sigma} = [\sigma_r, \sigma_\theta, \sigma_z, \sigma_{rz}]^T, \qquad \boldsymbol{\varepsilon} = [\varepsilon_r, \varepsilon_\theta, \varepsilon_z, \varepsilon_{rz}]^T \tag{2}$$

Components of stress and strain vectors are related to displacement vector components by the following relations

$$\varepsilon_r = \frac{\partial u_r}{\partial r}, \varepsilon_\theta = \frac{u_r}{r}, \varepsilon_z = \frac{\partial u_z}{\partial z}, \varepsilon_{rz} = \frac{\partial u_r}{\partial z} + \frac{\partial u_z}{\partial r} \tag{3}$$

Stress vector is expressed in terms of strain vector by means of Hook's law

$$\boldsymbol{\sigma} = \mathbf{D}\boldsymbol{\varepsilon} \tag{4}$$

For isotropic materials matrix $\mathbf{D}$ is defined as follows

$$\mathbf{D} = \frac{E(r)}{(1+\nu)(1-2\nu)}\begin{bmatrix} 1-\nu & \nu & \nu & 0 \\ \nu & 1-\nu & \nu & 0 \\ \nu & \nu & 1-\nu & 0 \\ 0 & 0 & 0 & \dfrac{(1-2\nu)}{2} \end{bmatrix} \tag{5}$$

Where, E and ν are modulus of elasticity and poison's ratio respectively. In this work for FGM cylinders, E is considered to be variable in radial direction and ν is considered to be constant.

3. Mesh-free numerical analysis

In these analyses moving least square (MLS) shape functions introduced by Lancaster *et al*. (1981) is used for approximation of displacement vector. In this approximation variable $u(\mathbf{X})$ in domain Ω in rz plane at point $\mathbf{X}$(r,z) is approximated as follows

$$u(\mathbf{X}) = \sum_{i=1}^{m} p_i(\mathbf{X})a_i = \mathbf{P}^{\mathrm{T}}(\mathbf{X})\mathbf{a}(\mathbf{X}) \tag{6}$$

Where $\mathbf{P}(\mathbf{X})$ is base vector and m is number of components of the base vector. For axisymmetric problems components of the linear and quadratic base vectors are defined as follows

$$\begin{aligned} P(X) &= [1, r, z]^T \\ P(X) &= [1, r, z, rz, r^2, z^2]^T \end{aligned} \tag{7}$$

Variable coefficients $a_i(X)$ are determined by minimizing the following weighted error norm

$$J = \sum_{i=1}^{n} w(\mathbf{X}-\mathbf{X}_i)[\mathbf{P}^{\mathrm{T}}(\mathbf{X}_i)\mathbf{a}(\mathbf{X}) - \hat{u}_i]^2 \tag{8}$$

Where n is the number of nodes in the support domain of the point X(r,z). At these nodes weight function w($\mathbf{X}$- $\mathbf{X}_\mathrm{i}$) is non zero. $\hat{u}_i$ is virtual nodal value at node $\mathrm{X_i}$. Minimization of J leads to

$$\mathbf{a}(\mathbf{X}) = [\mathbf{M}(\mathbf{X})]^{-1} \cdot \mathbf{B}(\mathbf{X}) \cdot \hat{\mathbf{u}} \tag{9}$$

Where $\mathbf{M}(\mathbf{X})$ (moment matrix) and $\mathbf{B}(\mathbf{X})$ are defined as follows

$$\mathbf{M}(\mathbf{X}) = \left[\sum_{i=1}^{n} w(\mathbf{X}-\mathbf{X}_i)\mathbf{P}(\mathbf{X}_i)\mathbf{P}^{\mathrm{T}}(\mathbf{X}_i)\right] \tag{10}$$

$$\mathbf{B}(\mathbf{X}) = [w(\mathbf{X}-\mathbf{X}_1)\mathbf{P}(\mathbf{X}_1), w(\mathbf{X}-\mathbf{X}_2)\mathbf{P}(\mathbf{X}_2), \ldots, w(\mathbf{X}-\mathbf{X}_n)\mathbf{P}(\mathbf{X}_n)] \tag{11}$$

$\hat{\mathbf{u}}$ is virtual nodal values vector and its components are defined as follows

$$\hat{\mathbf{u}} = [\hat{u}_1, \hat{u}_2, \ldots\ldots\ldots \hat{u}_n]^T \tag{12}$$

Substitution of Eq. (9) in Eq. (6) leads to

$$u(X) = \sum \Phi_i \hat{u}_i \tag{13}$$

Φ_i is MLS shape function of node located at $\mathbf{X}=\mathbf{X}_i$ and defined as follows

$$\Phi_i(\mathbf{X}) = \underbrace{\mathbf{P}^{\mathbf{T}}(\mathbf{X})[\mathbf{M}(\mathbf{X})]^{-1} w(\mathbf{X}-\mathbf{X}_i)\mathbf{P}(\mathbf{X}_i)}_{1\times 1} \tag{14}$$

In the present work cubic spline weight function is used in MLS shape functions. Displacement vector $\boldsymbol{u}$ in Eq. (1) can be approximated by MLS shape functions as follows

$$\mathbf{u} = [u_r, u_z]^T = \mathbf{\Phi}\hat{\mathbf{u}} \tag{15}$$

Where

$$\hat{\mathbf{u}} = [(\hat{u}_r)_1, (\hat{u}_z)_1, \ldots\ldots\ldots, (\hat{u}_r)_n, (\hat{u}_z)_n]^T \tag{16}$$

and

$$\mathbf{\Phi} = \begin{bmatrix} \Phi_1 & 0 & \Phi_2 & 0 & \ldots. & \Phi_n & 0 \\ 0 & \Phi_1 & 0 & \Phi_2 & \ldots. & 0 & \Phi_n \end{bmatrix} \tag{17}$$

By using Eq. (15) for approximation of displacement vector, strain vector can be expressed in terms of virtual nodal values

$$\boldsymbol{\varepsilon} = \mathbf{B}\hat{\mathbf{u}} \tag{18}$$

Where matrix $\mathbf{B}$ is defined as follows

$$\mathbf{B} = \begin{bmatrix} \frac{\partial \Phi_1}{\partial r} & 0 & \frac{\partial \Phi_2}{\partial r} & 0 & \ldots\ldots & \frac{\partial \Phi_n}{\partial r} & 0 \\ \frac{\Phi_1}{r} & 0 & \frac{\Phi_2}{r} & 0 & \ldots\ldots & \frac{\Phi_n}{r} & 0 \\ 0 & \frac{\partial \Phi_1}{\partial z} & 0 & \frac{\partial \Phi_2}{\partial z} & \ldots\ldots & 0 & \frac{\partial \Phi_n}{\partial z} \\ \frac{\partial \Phi_1}{\partial z} & \frac{\partial \Phi_1}{\partial r} & \frac{\partial \Phi_2}{\partial z} & \frac{\partial \Phi_2}{\partial r} & \ldots\ldots & \frac{\partial \Phi_n}{\partial z} & \frac{\partial \Phi_n}{\partial r} \end{bmatrix} \tag{19}$$

Substitution of Eq. (4), Eq. (15) and Eq. (18) in Eq. (1) leads to

$$\delta(\hat{\mathbf{u}})^T\left(\left(\int_\Omega \mathbf{B}^T\mathbf{D}\mathbf{B}\,dv\right)\hat{\mathbf{u}} - \delta(\hat{\mathbf{u}})^T\int_\Gamma \mathbf{\Phi}^T\mathbf{F}\,ds\right) = 0 \tag{20}$$

Eq. (20) should be satisfied for every arbitrary $\delta(\hat{\mathbf{u}})$. Therefore we have

$$\left(\int_\Omega \mathbf{B}^T\mathbf{D}\mathbf{B}\,dv\right)\hat{\mathbf{u}} - \int_\Gamma \mathbf{\Phi}^T\mathbf{F}\,ds = 0 \tag{21}$$

Or

$$\mathbf{K}\hat{\mathbf{U}} = \mathbf{f},\ \hat{\mathbf{U}} = [(\hat{u}_r)_1, (\hat{u}_z)_1, \ldots\ldots\ldots (\hat{u}_r)_N, (\hat{u}_Z)_N]^T \tag{22}$$

Where

$$\mathbf{k} = \int_\Omega \mathbf{B}^T\mathbf{D}\mathbf{B}\,dv,\ \mathbf{f} = \int_\Gamma \mathbf{\Phi}^T\mathbf{F}\,ds \tag{23}$$

and N is total number of nodes. For numerical integration, problem domain is discretized to a set of background cells with Gauss points inside each cell. Then global stiffness matrix $\mathbf{k}$ is obtained numerically by sweeping all Gauss points inside Ω. Similarly global force vector $\mathbf{f}$ is formed numerically in the same manner but by sweeping all gauss points on Γ.

Imposition of essential boundary conditions in the system of Eq. (22) is not possible. Because MLS shape functions don't satisfy the Kronecker delta property. In this work transformation method is used for imposition of essential boundary conditions. For this purpose transformation matrix is formed by establishing relation between nodal displacement vector $\mathbf{U}$ and virtual displacement vector $\hat{\mathbf{U}}$.

$$\mathbf{U} = \mathbf{T}\hat{\mathbf{U}} \tag{24}$$

Where

$$\mathbf{U} = [(u_r)_1, (u_z)_1, \ldots\ldots\ldots (u_r)_N, (u_z)_N]^T \tag{25}$$

and $\mathbf{T}$ is the transformation matrix.

$$\mathbf{T} = \begin{bmatrix} \Phi_1(\mathbf{x}_1) & 0 & \Phi_2(\mathbf{x}_1) & 0 & \ldots. & \Phi_N(\mathbf{x}_1) & 0 \\ 0 & \Phi_1(\mathbf{x}_1) & 0 & \Phi_2(\mathbf{x}_1) & \ldots. & 0 & \Phi_N(\mathbf{x}_1) \\ . & . & . & . & & . & . \\ . & . & . & . & & . & . \\ . & . & . & . & & . & . \\ . & . & . & . & & . & . \\ . & . & . & . & & . & . \\ . & . & . & . & & . & . \\ \Phi_1(\mathbf{x}_N) & 0 & \Phi_2(\mathbf{x}_N) & 0 & \ldots. & \Phi_N(\mathbf{x}_N) & 0 \\ 0 & \Phi_1(\mathbf{x}_N) & 0 & \Phi_2(\mathbf{x}_N) & \ldots. & 0 & \Phi_N(\mathbf{x}_N) \end{bmatrix} \tag{26}$$

By using Eq. (24) system of linear Eq. (22) can be rearranged to

$$\hat{\mathbf{k}}\mathbf{U} = \hat{\mathbf{f}}, \hat{\mathbf{k}} = \mathbf{T}^{-\mathrm{T}} \cdot \mathbf{k} \cdot \mathbf{T}^{-1}, \hat{\mathbf{f}} = \mathbf{T}^{-\mathrm{T}} \cdot \mathbf{f} \tag{27}$$

Where, $\mathbf{T}^{-\mathrm{T}} = (\mathbf{T}^{-1})^{\mathrm{T}}$. Eq.(27) is obtained by substitution of $\hat{\mathbf{U}} = \mathbf{T}^{-1}\mathbf{U}$ in Eq.(22) and multiplication of the resulted equation by $\mathbf{T}^{-\mathrm{T}}$. Now the essential B.Cs. can be enforced to the modified equations system, Eq. (27), easily like the finite element method.

4. Results and discussions

Two types of cylinders, subjected to internal pressure P are analyzed by the proposed mesh-free method, cylinders with infinite length and cylinders with finite length. In all of analyses Poisson's ratio is constant and equal to 0.3.

4.1. Cylinders with infinite length

For this type of cylinders in the first analysis, variation of modulus of elasticity is given by

$$E = E_i\left(\frac{r}{r_i}\right)^n, n = \ln\left(\frac{E_o}{E_i}\right)/\ln\left(\frac{r_o}{r_i}\right) \tag{28}$$

Where E_i and E_o are modulus of elasticity at inner and outer radius respectively. In this analysis ratio of outer radius to inner radius $\left(\frac{r_o}{r_i}\right)$ is equal to 2. Also numerical values $E_i = 200$ GPa and $E_o = 360$ GPa are used. Variation of normalized value of radial and hoop stresses verses normalized radial distance are shown in Fig. 1 and Fig. 2 respectively. Where normalized stress is defined as ratio of stress to internal pressure, P. As shown in these figures, results obtained from the mesh-free method are in good agreement with analytical solution introduced by Tutuncu and Temel (2009) and results obtained from FEM.

In the second analysis modulus of elasticity is given by

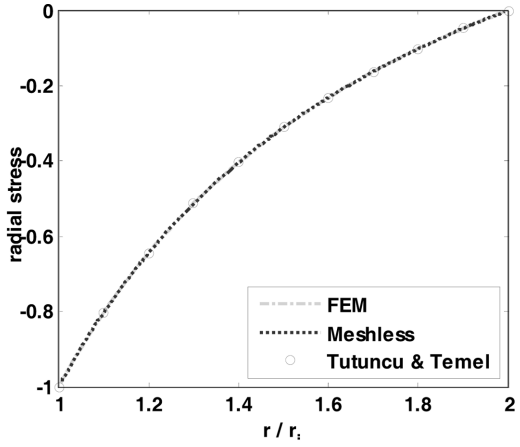

Fig. 1 Radial stress in the radial direction for the first model

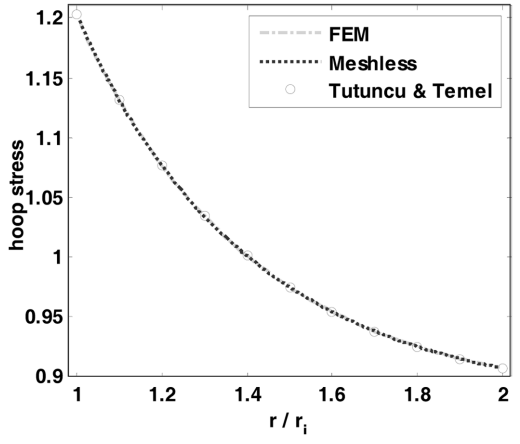

Fig. 2 Hoop stress in the radial direction for the first model

$$E = E_i + (E_o - E_i)\left(\frac{r^n - r_i^n}{r_o^n - r_i^n}\right) \tag{29}$$

Results obtained from this analysis are shown in Figs. 3-5. In these figures results of mesh-free method are compared with results of method introduced by Li and Peng (2009) and FEM. In the all of these figures good agreements are seen between them. In Fig. 3 effect of exponent n in Eq. (29) on hoop stress is shown for a cylinder with $\frac{r_i}{r_o} = 0.1$. This figure reveals that exponent n has a significant effect on hoop stress. As shown in this figure maximum value of hoop stress and its location are different for $n = 0.1$ and $n = 10$. Similar results for a cylinder with $\frac{r_i}{r_o} = 0.5$ are shown in Fig. 4. Comparison of Fig. 3 and Fig. 4 reveals that wall thickness of the FGM cylinder has a significant effect on hoop stress variation in radial direction. In the first case where $\frac{r_i}{r_o} = 0.1$, hoop stress decreases in the positive radial direction and its maximum value occurs at the inner radius. But for the second case where $\frac{r_i}{r_o} = 0.5$, hoop stress increases in the positive radial direction and its maximum value occurs at the outer radius. In Fig. 5 variation of radial stress is shown for the above mentioned cases. It is obvious from this figure that exponent n doesn't have a significant effects on radial stress. But for the case $\frac{r_i}{r_o} = 0.5$ radial stress vanishes more rapidly.

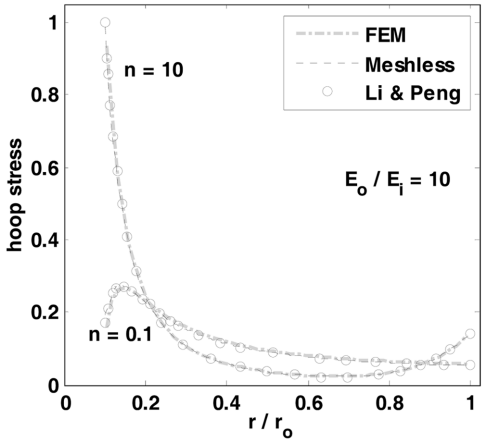

Fig. 3 Hoop stress in radial direction for the second model with $\frac{r_i}{r_o} = 0.1$

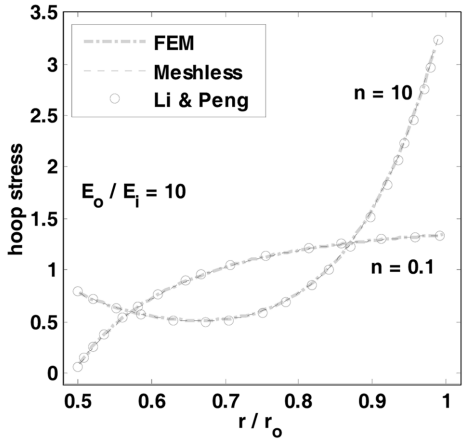

Fig. 4 Hoop stress in radial direction for the second model with $\frac{r_i}{r_o} = 0.5$

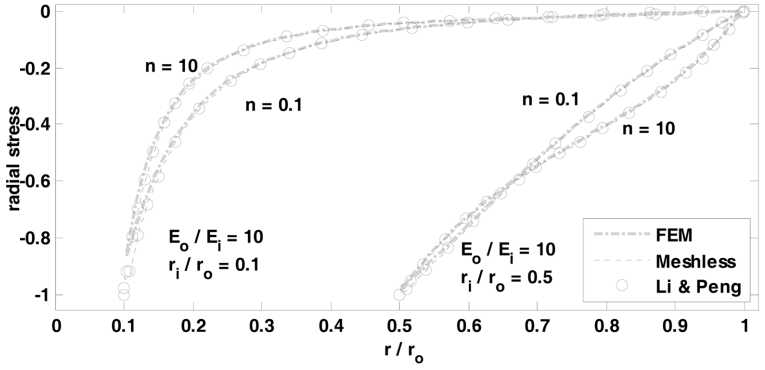

Fig. 5 Radial stress in radial direction for the second model

4.2. Cylinders with finite length

Hollow cylinders with length of L = **1** m, internal radius of $r_i = 0.8\ m$ and external radius of $r_o = 1\ m$ are considered in these analyses. In these analyses transformation method is used for imposition of essential boundary conditions. Eq. (29) is used for variation of modulus of elasticity with $E_i = 200$ GPa, $E_o = 360$ GPa and $n = 10$. For this type of cylinders two different set of boundary conditions are considered.

In the first model ends of cylinder are constrained in r and z directions and cylinder is subjected to an internal pressure P. In Figs. 6-8 contours of normalized stresses are shown for this analysis. It is obvious from these figures that a very good agreement exist between results of mesh-free method and finite element method.

Fig. 6 shows that maximum hoop stress occurs at the middle of outer surface, but as shown in Fig. 7, maximum axial stress occurs at the inner corners of the cylinder. Fig. 8 reveals that maximum Von Mises stress occurs at inner and outer corners of the cylinder. In order to investigate the effect of length on stress distribution, this simulation was carried out for several values of L. Normalized hoop stresses along the radial direction on the mid plane for different values of L / r_o are shown in Fig. 9. It is obvious from this figure that as the length gets longer, the results get close to the plane strain condition.

In the second model lower end of cylinder constrained in the axial direction and upper end is considered to be free. Cylinder is subjected to internal and external pressure, P. Other conditions of this model are

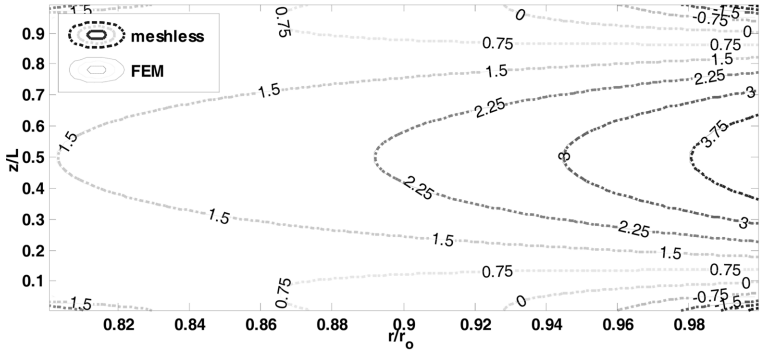

Fig. 6 Hoop stress distribution in the cylinder with finite length (first model)

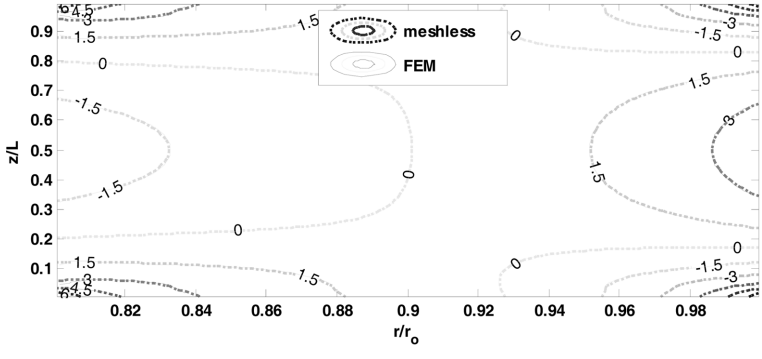

Fig. 7 Axial stress distribution in the cylinder with finite length (first model)

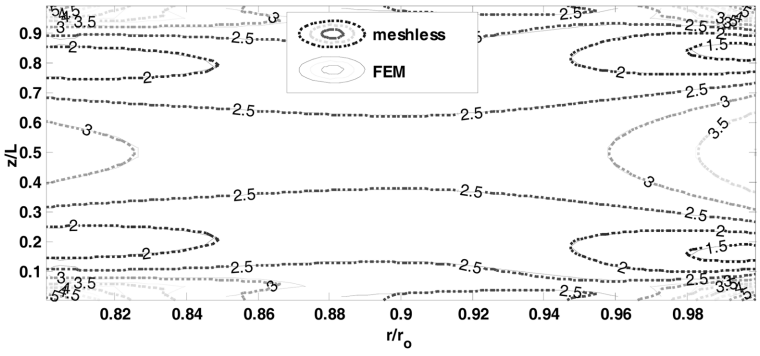

Fig. 8 Von Mises stress distribution in the cylinder with finite length (first model)

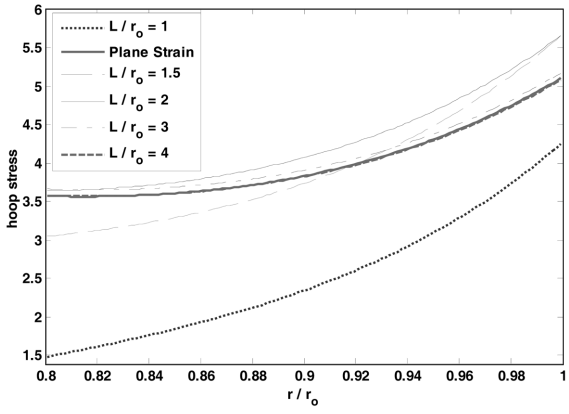

Fig. 9 Normalized hoop stress along the radial direction on mid plane for different values of L / r_o(first model)

considered to be the same as the first model. Results obtained for this model are shown in Figs. 10-12. In these figures a very good agreement is seen between results of mesh-free method and finite element method. Fig. 10 shows that hoop stress is negative in this model and varies from *-0.8P* to *-1.25P*. Axial stress is very low in comparison with the first model as seen in Fig. 11. This result is expected, because upper end is free in this model. For this model maximum Von Mises stress occurs at lower part of outer surface, as shown in Fig. 12. In order to investigate the effect of length on stress distribution, this simulation was carried out for several values of L. Normalized hoop stresses along the radial direction on the mid plane for different values of L / r_o are shown in Fig. 13. It is obvious from this figure that as the length gets longer, the results get close to the plane strain condition. Comparison of Fig.9 and Fig. 13 shows that plane strain condition is obtained more rapidly in the second model in comparison with the first one.

Results obtained from these models can be used in design procedure of FGM pressure vessels. These results can not be obtained by analytical methods.

5. Conclusions

In this work a mesh-free model was developed for static analysis of isotropic FGM cylinders. MLS shape functions were used for approximation of displacement field and transformation method was

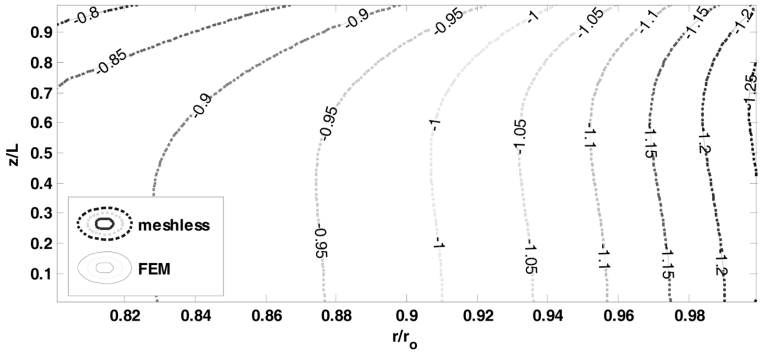

Fig. 10 Hoop stress distribution in the cylinder with finite length (second model)

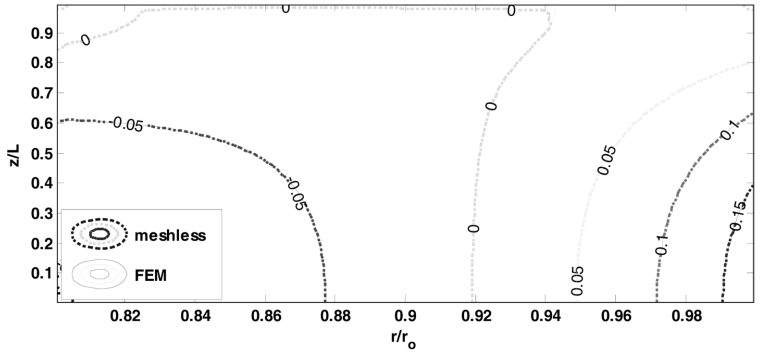

Fig. 11 Axial stress distribution in the cylinder with finite length (second model)

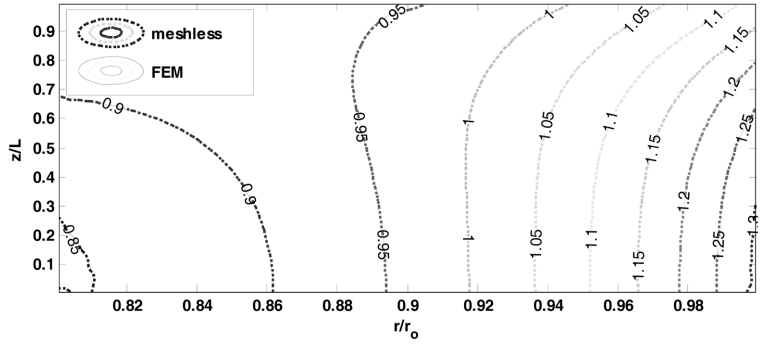

Fig. 12 Von Mises stress distribution in the cylinder with finite length (second model)

used for imposition of essential boundary conditions. Two types of FGM cylinders were analyzed by the proposed model, cylinders with infinite length and cylinders with finite length. Results obtained for cylinders with infinite length were compared with analytical solutions and a good agreement is seen between them. Then the proposed model was used for analysis of cylinders with finite length. Results obtained for cylinders with finite length were compared with those of the finite element analysis and a very good agreement was seen between them. These results can not be obtained easily by analytical methods. On the other hand stress field obtained by the finite element analysis is not continuous. But

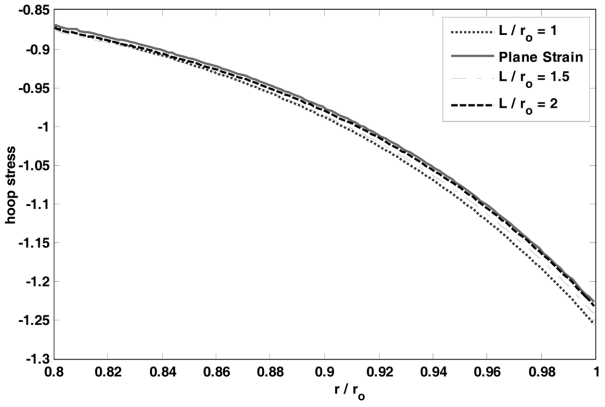

Fig. 13 Normalized hoop stress along the radial direction on mid plane for different values of L / r_o (second model)

stress field obtained from the mesh-free method is continuous. Therefore the proposed model can be used as an efficient tool in design procedure of FGM cylinders.

References

Askari, M., Akhlaghi, M. and Hosseini, S.M. (2009), "Dynamic analysis of two-dimensional functionally graded thick hollow cylinder with finite length under impact loading", *J. Acta. Mech.*, **208**(3-4), 163-180.

Ching, H.K. and Yen, S.C. (2005), "Meshless local Petrov-Galerkin analysis for 2d functionally graded elastic solids under mechanical and thermal loads", *J. Compos. Part B*, **36**(3), 223-240.

Gilhooley, D.F., Xiao, J.R., Batra, R.C., McCarthy, M.A. and Gillespie, Jr.J.W. (2008), "Two-dimensional stress analysis of functionally graded solids using the MLPG method with radial basis functions" *J. compu. mater. sci.*, **41**(4), 467-481.

Horgan, C.O. and Chan, A.M. (1999), "The pressurized hollow cylinder or disk problem for functionally graded isotropic linearly elastic materials", *J. Elasticity,* **55**(1), 43-59.

Jabbari, M., Bahtui, A. and Eslami, M.R. (2006), "Axisymmetric mechanical and thermal stresses in thick long FGM cylinders", *J. Therm. Stresses.*, **29**(7), 643-663.

Lancaster, P. and Salkauskas, K. (1981), "Surface generated by moving least squares methods", *Math. Comput.*, **37**(155), 141-158.

Li, X.-F. and Peng, X.-L. (2009), "A pressurized functionally graded hollow cylinder with arbitrarily varying material properties", *J. Elas.*, **96**(1), 81-95.

Sladek, J., Sladek, V. and Zhang. Ch. (2003), "Transient heat conduction analysis in functionally graded materials by the meshless local boundary integral equation method", *J. compu. mater. sci.*, **28**(3-4), 494-504.

Sladek, V., Sladek, J. and Zhang, Ch. (2008), "Local integral equation formulation for axially symmetric problems involving elastic FGM", *Eng. Anal. Bound. Elem.*, **32**(12), 1012-1024.

Tutuncu, N. and Ozturk, M. (2001), "Exact solutions for stresses in functionally graded pressure vessels", *J. Compos. part B,* **32**(8), 683-686.

Tutuncu, N. (2007), "Stresses in thick-walled FGM cylinders with exponentially-varying properties", *J. Eng. struct.*, **29**(9), 2032-2035.

Tutuncu, N. and Temel, B. (2009), "A novel approach to stress analysis of pressurized FGM cylinders, disks and spheres", *J. Compos. Struct.*, **91**(3), 385-390.

Zhao, X. and Liew, K.M. (2010), "A mesh-free method for analysis of the thermal and mechanical buckling of functionally graded cylindrical shell panels", *Comput. Mech.*, **45**, 297-310.